Draft version May 28, 2021
Typeset using LaTeX **twocolumn** style in AASTeX63

The Aligned Orbit of the Eccentric Warm Jupiter K2-232 b

Songhu Wang,[1] Joshua N. Winn,[2] Brett C. Addison,[3] Fei Dai,[4] Malena Rice,[5] Bradford Holden,[6] Jennifer A. Burt,[7] Xian-Yu Wang,[8,9] R. Paul Butler,[10] Steven S. Vogt,[6] and Gregory Laughlin[5]

[1] *Department of Astronomy, Indiana University, Bloomington, IN 47405*
[2] *Department of Astrophysical Sciences, Princeton University, 4 Ivy Lane, Princeton, NJ 08544*
[3] *University of Southern Queensland, Centre for Astrophysics, West Street, Toowoomba, QLD 4350 Australia*
[4] *Division of Geological and Planetary Sciences 1200 E California Blvd, Pasadena, CA 91125*
[5] *Department of Astronomy, Yale University, New Haven, CT 06511*
[6] *UCO/Lick Observatory, Department of Astronomy and Astrophysics, University of California at Santa Cruz,Santa Cruz, CA 95064*
[7] *Jet Propulsion Laboratory, California Institute of Technology, 4800 Oak Grove drive, Pasadena CA 91109*
[8] *National Astronomical Observatories, Chinese Academy of Sciences, Beijing 100012, China*
[9] *University of Chinese Academy of Sciences, Beijing, 100049, China*
[10] *Earth and Planets Laboratory, Carnegie Institution for Science, 5241 Broad Branch Road, NW, Washington, DC 20015*

(Received ?; Revised ?; Accepted ?)

AAS

ABSTRACT

0.26. $\lambda = -11.1 \pm 6.6°$.

Keywords: (1243), (490), (2177), (498), (1258), (484)

1. INTRODUCTION

6° (2012)

1796).

sw121@iu.edu

(Rø 1924; 1924)

2010; 2012).

1. 1996; 2008),

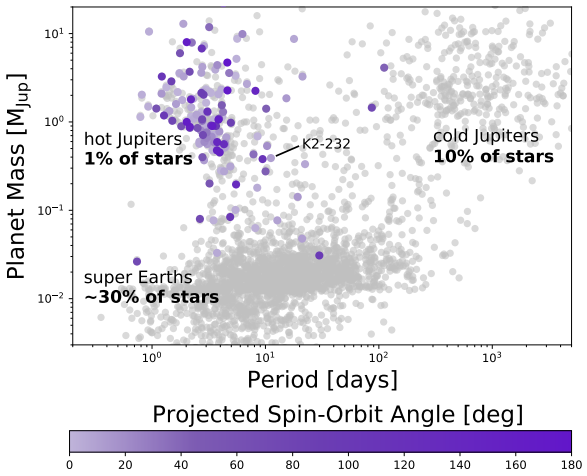

Figure 1. An up-to-date mass-period diagram of currently known exoplanets. Planets with Rossiter-McLaughlin (including Doppler tomography) measurements drawn from the TEPCat catalog (Southworth 2011) are shown as points color-coded by their observed spin-orbit angles, while planets without stellar obliquity measurements are depicted as gray dots. The majority of planets with existing Rossiter-McLaughlin measurements are hot Jupiters, which span a wide range of stellar obliquities. In this work, we have expanded the list of spin-orbit measurements to include a new warm Jupiter system: K2-232.

[illegible] (W[illegible] & M[illegible] 2003; F[illegible] & [illegible] 2007; N[illegible] 2016), [illegible] (W[illegible] & L[illegible] 2011; P[illegible] 2015).

2. O[illegible] *unrelated* [illegible] (B[illegible] et al. 2010), [illegible] (R[illegible] et al. 2012), [illegible] (L[illegible] et al. 2011), [illegible] (B[illegible] et al. 2011; [illegible] et al. 2014).

[illegible] 10 [illegible] — [illegible] (D[illegible] et al. 2013). [illegible]

[illegible] Jupiters [illegible]

F[illegible]

A[illegible] Rossiter-McLaughlin [illegible] Rossiter-McLaughlin [illegible]

H[illegible] Rossiter-McLaughlin [illegible] K2-232 b, [illegible] 0.39 $M_{\rm Jup}$ [illegible] 1.06 $R_{\rm Jup}$ [illegible] 11.17-[illegible] 0.26 (B[illegible] et al. 2018; Y[illegible] et al. 2018). In [illegible] (§2), [illegible] (§3), [illegible] (§4).

2. OBSERVATIONS

K2-232 [illegible] A[illegible] P[illegible] F[illegible] (APF) [illegible] (V[illegible] et al. 2014) [illegible] 29 October 2019 [illegible] 04 January 2020, [illegible] K2-232 b [illegible] 20-[illegible] APF's $1 \times 3''$ [illegible] 90,000. [illegible] APF [illegible] 5000–6200 Å [illegible] (PSF). [illegible] 2630 [illegible] 1494 [illegible] 1.52″ [illegible] 1.98″ [illegible]

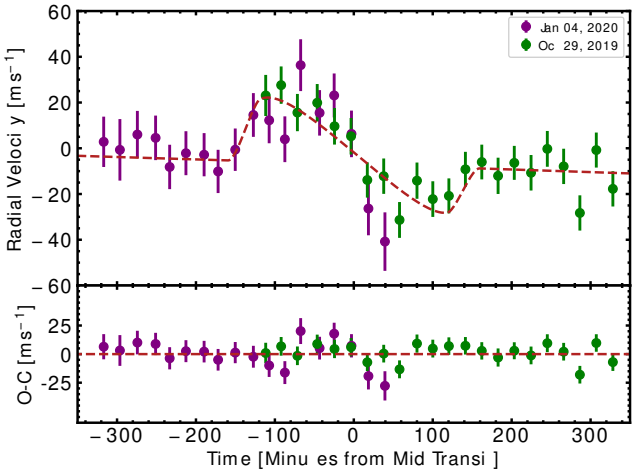

Figure 2. Spectroscopic radial velocities of K2-232 measured with the APF, as a function of orbital phase (minutes from mid-transit) along with the best-fitting Rossiter-McLaughlin model (red-dashed line). The radial velocity offsets in each of the datasets have been removed prior to fitting the combined and phased data. The green and maroon points are the radial velocities from the 29 October 2019 and 4 January 2020 transit observations, respectively. The lower panel shows the residuals between the observed data and the best-fitting model. The small structures remaining in the residuals are likely caused by stellar noise and variations in atmospheric extinction due to the presence of clouds at the end of night on 4 January 2020

.

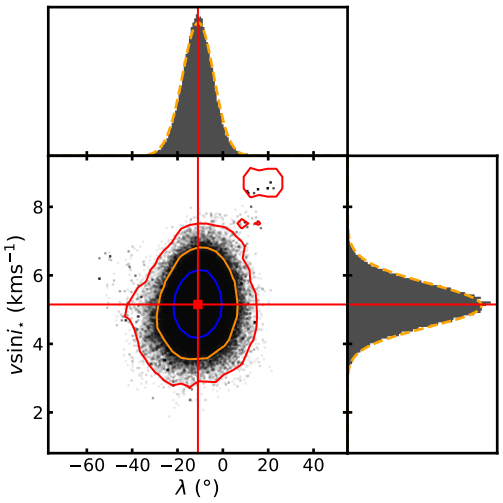

Figure 3. Posterior distributions of the projected spin-orbit angle (λ) and projected stellar rotational velocity ($v \sin i_\star$) for K2-232 from the Markov Chain Monte Carlo Rossiter-McLaughlin simulation. The posterior points inside the blue, yellow, and red contours lie within the 1σ, 2σ, and 3σ confidence regions, respectively. We have marginalized over λ and $v \sin i_\star$ and fit each with a Gaussian. The red square denotes the preferred model solution for λ and $v \sin i_\star$ as given in Table 2.

3. SPIN-ORBIT ANGLE DETERMINATION

[1] https://github.com/MNGuenther/allesfitter

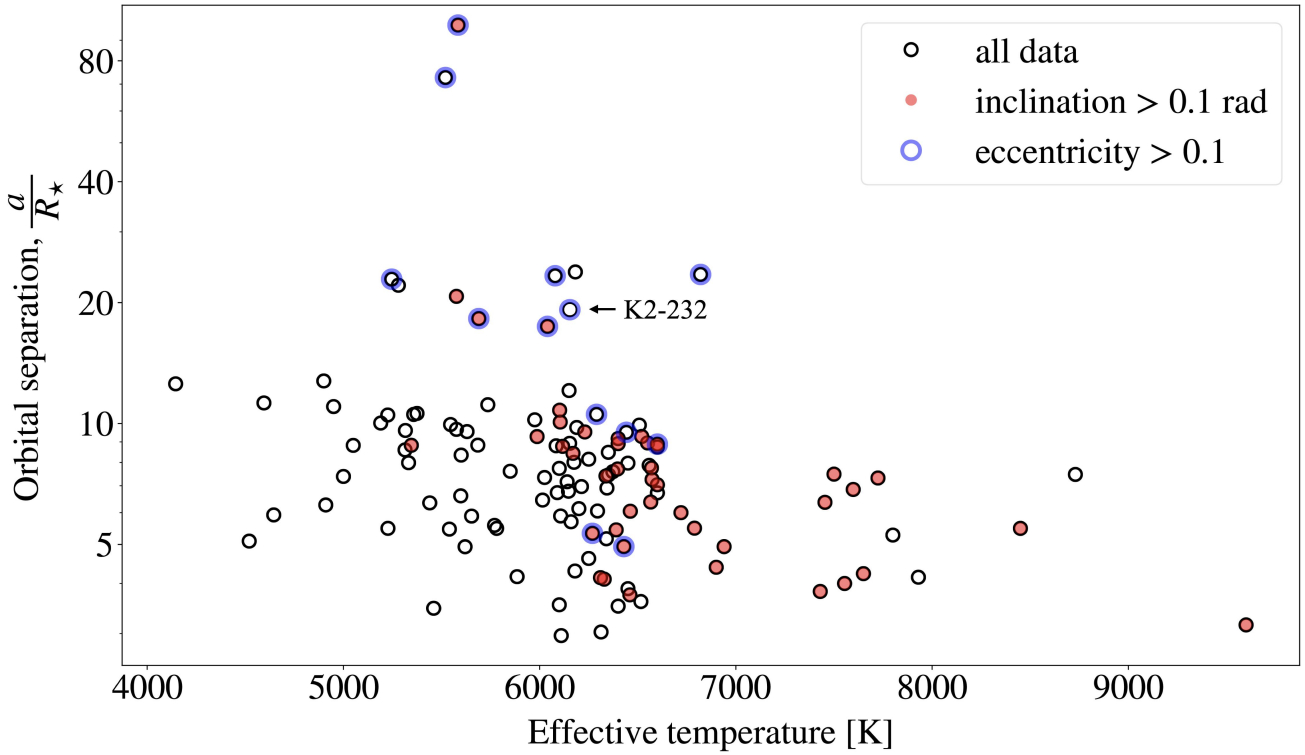

Figure 4. Key variables that may affect tidal dissipation rates, provided for all the transiting giant planets ($M_{\rm p} > 0.3\,M_{\rm Jup}$) for which the Rossiter-McLaughlin effect has been reported. The horizontal axis shows effective temperature of the host star, and the vertical axis shows the dimensionless orbital separation (semimajor axis divided by stellar radius). Red points indicate the sky-projected obliquity exceeds 0.1 rad (5.7 deg), and blue encircled points indicate the orbital eccentricity exceeds 0.1, in both cases with at least 3-σ confidence. The scarcity of misaligned or eccentric systems with $a/R_\star \lesssim 10$ and $T_{\rm eff} \lesssim 6000\,$K suggests that tidal effects have damped the obliquity and eccentricity of at least some of those systems.

∼ 6 ±1000 −1. 2 λ, $v \sin i_\star$,
1σ (2018) (2018).
$K2$ λ $v \sin i_\star$ $v \sin i_\star$
MCMC (MCMC)
100 300,000
$(a \cos i/R_\star \approx 0.5)$ K2-232 b(& 2007). $v \sin i_\star$ (∼ 12%) λ.

...ed ... $\lambda = -11.1 \pm 6.6°$ ... $v \sin i_* = 5.15 \pm 0.62$ ... $^{-1}$, ... K2-232 ...

4. DISCUSSION

... $a/R_\star \lesssim 10$) ... $T_{\rm eff} \lesssim$ 6,000 K) ... $a/R_\star$ ... $T_{\rm eff}$ ... λ ... [2] ... $M_{\rm Jup}$). ... σ ... 0.1 ... ($5.7 °) ... σ ... K2-232, ... $a/R_\star \approx 19$ ... $T_{\rm eff} \approx 6154$ K. ... *all* ... $a/R_\star \lesssim 10$ ... $T_{\rm eff} \lesssim 6000$ K ...

[2] https://www.astro.keele.ac.uk/jkt/tepcat/

Table 1. Radial velocities for the K2-232 system collected with the APF in this work

Time (BJD)	RV $(\mathrm{m\,s^{-1}})$	σ_{RV} $(\mathrm{m\,s^{-1}})$
Oct. 29, 2019		
2458785.76135	54.43	6.22
2458785.77494	58.95	4.97
2458785.78924	46.95	4.93
2458785.80668	51.24	5.0
2458785.82189	40.96	4.69
2458785.83645	36.59	4.67
2458785.85075	17.47	4.15
2458785.86519	19.14	4.21
2458785.8791	0.0	4.39
2458785.89446	17.18	4.55
2458785.90838	9.12	4.32
2458785.92253	10.52	4.06
2458785.93707	22.14	4.04
2458785.95148	25.33	3.95
2458785.96582	19.29	4.56
2458785.98007	24.96	3.62
2458785.99483	20.63	4.26
2458786.00914	31.08	4.38
2458786.02352	23.42	4.19
2458786.03779	3.06	4.16
2458786.05224	30.56	4.07
2458786.06682	13.6	4.18
Jan. 4, 2020		
2458852.62955	9.26	7.32
2458852.64381	5.75	10.65
2458852.65918	12.45	6.25
2458852.67522	10.99	5.22
2458852.68760	-1.73	5.16
2458852.70191	4.28	4.99
2458852.71790	3.62	4.65
2458852.73021	-3.69	4.68
2458852.74530	5.81	4.29
2458852.76125	20.99	4.89
2458852.77514	18.67	5.77
2458852.78896	10.38	5.71
2458852.80286	42.77	7.80
2458852.81951	21.92	5.60
2458852.83234	29.54	4.96
2458852.84758	12.73	6.02
2458852.86249	-19.92	8.31
2458852.87701	-34.37	9.8

ACKNOWLEDGMENTS

[illegible] N. G[illegible] ü[illegible] [illegible] `Allesfitter` [illegible] [illegible] J.N.W[illegible] H[illegible] M.R. [illegible] N[illegible] G[illegible] R[illegible] P[illegible] G[illegible] N[illegible] DGE-1752134. W[illegible] M[illegible] P[illegible] J[illegible] P[illegible] L[illegible] C[illegible] I[illegible] T[illegible] N[illegible] A[illegible] S[illegible] A[illegible] (80NM0018D0004). [illegible] C[illegible] N[illegible] A[illegible] D[illegible] C[illegible] (NADC), C[illegible] V[illegible] O[illegible] (C[illegible] V[illegible]), A[illegible] B[illegible] D[illegible] J[illegible] R[illegible] C[illegible] N[illegible] A[illegible] O[illegible], C[illegible] A[illegible] S[illegible] A[illegible] C[illegible]

REFERENCES

Table 2. System Parameters, Priors, and Results for K2-232

Parameter	Priors[a]	Results 29 Oct. 2019	Results 4 Jan. 2020	Preferred Solution Results combined transits
Fitted Parameters:				
Orbital period, P (days)	$10; 11.168454; 12$	11.168452 ± 0.000025	11.168466 ± 0.000024	11.168455 ± 0.000023
Mid-transit epoch (2450000-BJD), T_0	7825.3[b]	8305.59490 ± 0.00099	8339.1008 ± 0.0010	8339.10040 ± 0.0010
Cosine of the orbital inclination, $\cos i$	$0; 0.015; 1$	$0.0345^{+0.0028}_{-0.0024}$	$0.0344^{+0.0029}_{-0.0024}$	$0.0344^{+0.0028}_{-0.0023}$
Planet-to-star radius ratio, $R_P/R_\star$	$0; 0.08868; 1$	$0.09142^{+0.00052}_{-0.00049}$	$0.09138^{+0.00052}_{-0.00048}$	$0.09140^{+0.00051}_{-0.00048}$
Sum of radii divided by the orbital semimajor axis, $(R_\star + R_P)/a$	$0; 0.05654; 1$	$0.0676^{+0.0026}_{-0.0023}$	$0.0676^{+0.0027}_{-0.0023}$	$0.0675^{+0.0026}_{-0.0022}$
RV semi-amplitude, K ($\mathrm{m\ s^{-1}}$)	$0; 33; 1000$	32.4 ± 2.5	32.3 ± 2.6	32.4 ± 2.5
Eccentricity parameter 1, $\sqrt{e}\cos\omega$	$-1.0; -0.453; 1.0$	$-0.441^{+0.035}_{-0.030}$	$-0.440^{+0.036}_{-0.031}$	$-0.440^{+0.035}_{-0.030}$
Eccentricity parameter 2, $\sqrt{e}\sin\omega$	$-1.0; -0.231; 1.0$	$-0.217^{+0.076}_{-0.061}$	$-0.217^{+0.081}_{-0.062}$	$-0.221^{+0.074}_{-0.060}$
Limb-darkening coefficient 1, q_1	$0; 0.5; 1.0$	0.538 ± 0.068	0.544 ± 0.067	0.540 ± 0.068
Limb-darkening coefficient 2, q_2	$0; 0.5; 1.0$	$0.187^{+0.054}_{-0.043}$	$0.183^{+0.054}_{-0.041}$	$0.185^{+0.054}_{-0.043}$
Stellar rotation velocity, $v \sin i_\star$ ($\mathrm{km\ s^{-1}}$)	$0; 5; 10$	5.23 ± 0.72	$5.5^{+1.8}_{-1.6}$	5.15 ± 0.62
Projected spin-orbit angle, λ (deg)	$-180; 0; 180$	-14.5 ± 7.7	-2^{+12}_{-16}	-11.1 ± 6.6
Relative RV Offset for in-transit APF, Oct. 29 2019 ($\mathrm{m\,s^{-1}}$)	$-1000; 0; 1000$	32.0 ± 3.1	...	32.8 ± 2.8
Relative RV Offset for in-transit APF, Jan. 4 2020 ($\mathrm{m\,s^{-1}}$)	$-1000; 0; 1000$	...	8.6 ± 4.3	$7.1^{+3.2}_{-3.5}$
Relative RV Offset for out-of-transit APF ($\mathrm{m\,s^{-1}}$)	$-1000; 0; 1000$	-98.7 ± 1.9	$98.7^{+1.9}_{-1.8}$	$-98.7^{+1.9}_{-1.7}$
Relative RV Offset for Coralie ($\mathrm{m\,s^{-1}}$)	$-1000; 0; 1000$	-57^{+19}_{-22}	-57^{+19}_{-22}	-58^{+19}_{-22}
Relative RV Offset for FEROS ($\mathrm{m\,s^{-1}}$)	$-1000; 0; 1000$	3.5 ± 2.1	3.4 ± 2.1	3.5 ± 2.1
Relative RV Offset for HARPS ($\mathrm{m\,s^{-1}}$)	$-1000; 0; 1000$	-0.7 ± 2.7	$-0.6^{+2.7}_{-2.5}$	$-0.8^{+2.7}_{-2.5}$
Derived Parameters:				
Planetary radius R_b ($\mathrm{R_{jup}}$)	...	$0.380^{+0.049}_{-0.044}$	$0.378^{+0.049}_{-0.045}$	$0.378^{+0.047}_{-0.045}$
Planetary Mass M_b ($\mathrm{M_{jup}}$)	...	1.097 ± 0.025	1.096 ± 0.025	1.097 ± 0.024
Impact parameter b	...	0.587 ± 0.014	0.586 ± 0.013	0.587 ± 0.013
Transit duration T_{14} (h)	...	5.2893 ± 0.010	5.2893 ± 0.010	5.2895 ± 0.0099
Transit depth δ	...	0.009331 ± 0.000019	0.009330 ± 0.000018	$0.009330^{+0.000019}_{-0.000021}$
Inclination i ($^\circ$)	...	$88.02^{+0.14}_{-0.16}$	$88.03^{+0.14}_{-0.17}$	$88.03^{+0.13}_{-0.16}$
Eccentricity e	...	$0.245^{+0.020}_{-0.022}$	$0.246^{+0.020}_{-0.022}$	$0.247^{+0.020}_{-0.021}$
Argument of periastron ω (deg)	...	$206.3^{+8.0}_{-9.4}$	$206.3^{+7.8}_{-9.8}$	$206.7^{+7.8}_{-9.0}$
Limb darkening; u_1	...	$0.276^{+0.061}_{-0.053}$	$0.272^{+0.058}_{-0.052}$	$0.273^{+0.059}_{-0.053}$
Limb darkening; u_2	...	$0.461^{+0.098}_{-0.10}$	$0.468^{+0.096}_{-0.10}$	$0.464^{+0.097}_{-0.10}$

[a] The uniform priors are presented in the form of three numbers: the first number is the lower bound, the middle number is the initial guess, and the last number is the upper bound.

[b] We provided a reference mid-transit epoch for T_0. During the fit, `Allesfitter` can shift epochs to the data center to derive an optimal T_0.

Albrecht, S., Winn, J. N., Johnson, J. A., et al. 2012, ApJ, 757, 18

Bate, M. R., Lodato, G., & Pringle, J. E. 2010, MNRAS, 401, 1505

Batygin, K., Morbidelli, A., & Tsiganis, K. 2011, A&A, 533, A7

Brahm, R., Espinoza, N., Jordán, A., et al. 2018, MNRAS, 477, 2572

Butler, R. P., Marcy, G. W., Williams, E., et al. 1996, PASP, 108, 500

de Laplace, P. S. 1796, Exposition du système du monde, doi:10.3931/e-rara-497

Dong, S., Katz, B., & Socrates, A. 2013, The Astrophysical Journal Letters, 781, L5

Fabrycky, D., & Tremaine, S. 2007, ApJ, 669, 1298

Ford, E. B., & Rasio, F. A. 2008, ApJ, 686, 621

Gaudi, B. S., & Winn, J. N. 2007, ApJ, 655, 550

Gaudi, B. S., Stassun, K. G., Collins, K. A., et al. 2017, Nature, 546, 514

Goldreich, P., & Sari, R. 2003, ApJ, 585, 1024

Günther, M. N., & Daylan, T. 2020, arXiv e-prints, arXiv:2003.14371

Innanen, K. A., Zheng, J. Q., Mikkola, S., & Valtonen, M. J. 1997, AJ, 113, 1915

Kant, I. 1755, Allgemeine Naturgeschichte und Theorie des Himmels

Lai, D., Foucart, F., & Lin, D. N. C. 2011, MNRAS, 412, 2790

McLaughlin, D. 1924, The Astrophysical Journal, 60

Naoz, S. 2016, ARA&A, 54, 441

Narita, N., Hirano, T., Sato, B., et al. 2009, PASJ, 61, 991

Petrovich, C. 2015, ApJ, 799, 27

Pont, F., Endl, M., Cochran, W. D., et al. 2010, MNRAS, 402, L1

Queloz, D., Anderson, D. R., Collier Cameron, A., et al. 2010, A&A, 517, L1

Rasio, F. A., & Ford, E. B. 1996, Science, 274, 954

Rogers, T. M., Lin, D. N. C., & Lau, H. H. B. 2012, ApJL, 758, L6

Rossiter, R. 1924, The Astrophysical Journal, 60

Souami, D., & Souchay, J. 2012, A&A, 543, A133

Southworth, J. 2011, MNRAS, 417, 2166

Storch, N. I., Anderson, K. R., & Lai, D. 2014, Science, 345, 1317

Vogt, S. S., Radovan, M., Kibrick, R., et al. 2014, PASP, 126, 359

Winn, J. N., Fabrycky, D., Albrecht, S., & Johnson, J. A. 2010, ApJL, 718, L145

Winn, J. N., Johnson, J. A., Albrecht, S., et al. 2009a, ApJL, 703, L99

Winn, J. N., Johnson, J. A., Peek, K. M. G., et al. 2007, ApJL, 665, L167

Winn, J. N., Howard, A. W., Johnson, J. A., et al. 2009b, ApJ, 703, 2091

Wu, Y., & Lithwick, Y. 2011, ApJ, 735, 109

Wu, Y., & Murray, N. 2003, ApJ, 589, 605

Yu, L., Rodriguez, J. E., Eastman, J. D., et al. 2018, AJ, 156, 127